NERC
NORTH AMERICAN ELECTRIC RELIABILITY CORPORATION

Benchmark Geomagnetic Disturbance Event Description

Project 2013-03 GMD Mitigation
Standard Drafting Team
Draft: June 10, 2014

RELIABILITY | ACCOUNTABILITY

Table of Contents

Preface

The North American Electric Reliability Corporation (NERC) is a not-for-profit international regulatory authority whose mission is to ensure the reliability of the Bulk-Power System (BPS) in North America. NERC develops and enforces Reliability Standards; annually assesses seasonal and long-term reliability; monitors the BPS through system awareness; and educates, trains, and certifies industry personnel. NERC's area of responsibility spans the continental United States, Canada, and the northern portion of Baja California, Mexico. NERC is the electric reliability organization (ERO) for North America, subject to oversight by the Federal Energy Regulatory Commission (FERC) and governmental authorities in Canada. NERC's jurisdiction includes users, owners, and operators of the BPS, which serves more than 334 million people.

The North American BPS is divided into several assessment areas within the eight Regional Entity (RE) boundaries, as shown in the map and corresponding table below.

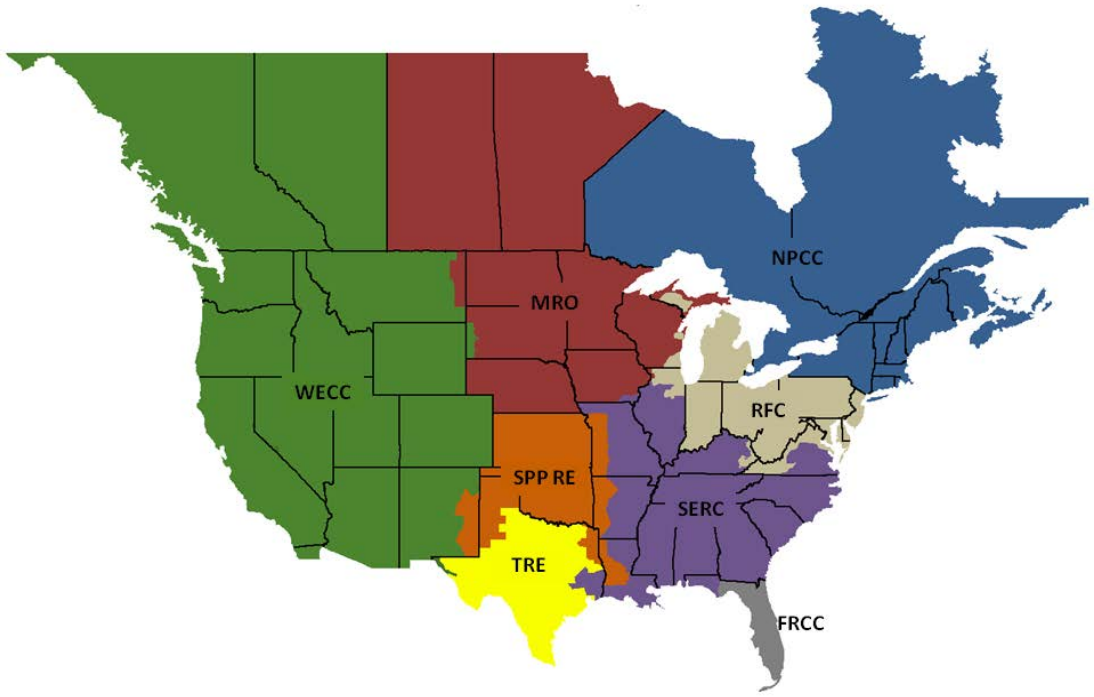

FRCC	Florida Reliability Coordinating Council
MRO	Midwest Reliability Organization
NPCC	Northeast Power Coordinating Council
RFC	Reliability*First* Corporation
SERC	SERC Reliability Corporation
SPP-RE	Southwest Power Pool Regional Entity
TRE	Texas Reliability Entity
WECC	Western Electric Coordinating Council

Introduction

Background

The purpose of the benchmark geomagnetic disturbance (GMD) event description is to provide a defined event for assessing system performance during a low probability, high magnitude GMD event as required by proposed standard TPL-007-1 – Transmission System Planned Performance for Geomagnetic Disturbance Events. The benchmark GMD event defines the geoelectric field values used to compute geomagnetically-induced current (GIC) flows for a GMD Vulnerability Assessment.

On May 16, 2013, FERC issued Order No. 779, directing NERC to develop Standards that address risks to reliability caused by geomagnetic disturbances in two stages:

- Stage 1 Standard(s) that require applicable entities to develop and implement Operating Procedures. EOP-010-1 – Geomagnetic Disturbance Operations is pending at FERC in Docket No. RM14-1-000.
- Stage 2 Standard(s) that require applicable entities to conduct assessments of the potential impact of benchmark GMD events on their systems. If the assessments identify potential impacts, the Standard(s) will require the applicable entity to develop and implement a plan to mitigate the risk.

TPL-007-1 is a new Reliability Standard developed to specifically address the Stage 2 directives in Order No. 779. The benchmark GMD event will define the scope of the Stage 2 Reliability Standard.

General Characteristics

The benchmark GMD event described herein takes into consideration the known characteristics of a severe GMD event and its impact on an interconnected transmission system. These characteristics include:

- Geomagnetic Latitude – The amplitude of the induced geoelectric field for a given GMD event is reduced as the observation point moves away from the earth's magnetic poles.
- Earth Conductivity – The amplitude and phase of the geoelectric field depends on the local or regional earth ground resistivity structure. Higher geoelectric field amplitudes are induced in areas of high resistivity.
- Transformer Electrical Response – Transformers can experience half-cycle saturation when subjected to GIC. Transformers under half-cycle saturation absorb increased amounts of reactive power (var) and inject harmonics into the system. However, half-cycle saturation does not occur instantaneously and depends on the electrical characteristics of the transformer and GIC amplitude [1]. Thus, the effects of transformer reactive power absorption and harmonic generation do not occur instantaneously, but instead may take up to several seconds. It is conservative, therefore, to assume that the effects of GIC on transformer var absorption and harmonic generation are instantaneous.
- Transformer Thermal Effects (e.g. hot spot transformer heating) – Heating of the winding and other structural parts can occur in power transformers during a GMD event. However, the thermal impacts are not instantaneous and are dependent on the thermal time constants of the transformer. Thermal time constants for hot spot heating in power transformers are in the 5-20 minute range.
- Geoelectric Field Waveshape – The geoelectric field waveshape has a strong influence on the hot spot heating of transformer windings and structural parts since thermal time constants of the transformer and time to peak of storm maxima are both on the order of minutes. The frequency content of the magnetic field (dB/dt) is a function of the waveshape, which in turn has a direct effect on the geoelectric field since the earth response to external dB/dt is frequency-dependent.
- Wide Area Geomagnetic Phenomena – The influence of GMD events is typically over a very broad area (e.g. continental scale); however, there can be pockets or very localized regions of enhanced geomagnetic activity. Since geomagnetic disturbance impacts within areas of influence of approximately 100-200 km do not have a widespread impact on the interconnected transmission system (see Appendix I), statistical methods used to assess the frequency of occurrence of a severe GMD event need to consider broad geographical regions to avoid bias caused by spatially localized geomagnetic phenomena.

Benchmark GMD Event Description

Severe geomagnetic disturbance events are high-impact, low-frequency (HILF) events [2]; thus, any benchmark event should consider the probability that the event will occur, as well as the impact or consequences of such an event. The benchmark event is composed of the following elements: 1) a reference peak geoelectric field amplitude (V/km) derived from statistical analysis of historical magnetometer data; 2) scaling factors to account for local geomagnetic latitude; 3) scaling factors to account for local earth conductivity; and 4) a reference geomagnetic field time series or waveshape to facilitate time-domain analysis of GMD impact on equipment.

Reference Geoelectric Field Amplitude

The reference geoelectric field amplitude was determined through statistical analysis using the plane wave method [3]-[10] geomagnetic field measurements from geomagnetic observatories in northern Europe [11] and the reference (Quebec) earth model shown in **Table 1** [12]. For details of the statistical considerations, see Appendix I. The Quebec earth model is generally resistive and the geological structure is relatively well understood.

Table 1: Reference earth model (Quebec)

Thickness (km)	Resistivity (Ω-m)
15	20,000
10	200
125	1,000
200	100
∞	3

The statistical analysis (see Appendix II) resulted in a conservative peak geoelectric field amplitude of approximately 8 V/km. For steady-state GIC and load flow analysis, the direction of the geoelectric field is assumed to be variable meaning that it can be in any direction (Eastward, Northward, or a vectorial combination thereof).

The frequency of occurrence of this benchmark GMD event is estimated to be approximately 1 in 100 years (see Appendix I). The selected frequency of occurrence is consistent with utility practices where a design basis frequency of 1 in 50 years is currently used as the storm return period for determining wind and ice loading of transmission infrastructure [13], for example.

The regional geoelectric field peak amplitude, E_{peak}, to be used in calculating GIC in the GIC system model can be obtained from the reference value of 8 V/km using the following relationship

$$E_{peak} = 8 \times \alpha \times \beta \text{ (V/km)} \quad (1)$$

where α is the scaling factor to account for local geomagnetic latitude, and β is a scaling factor to account for the local earth conductivity structure (see Appendix II).

Reference Geomagnetic Field Waveshape

The reference geomagnetic field waveshape was selected after analyzing a number of recorded GMD events, including the reference storm of the NERC interim report of 2012 [14], measurements at the Nurmijarvi (NUR) and Memanbetsu (MMB) geomagnetic observatories for the "Halloween event" of October 29-31, 2003, and the March 1989 GMD event that caused the Hydro Quebec blackout. The geomagnetic field measurement record of the March 13-14 1989 GMD event, measured at NRCan's Ottawa geomagnetic observatory, was selected as the

reference geomagnetic field waveform because it provides generally conservative results when performing thermal analysis of power transformers (see Appendix I). The reference geomagnetic field waveshape is used to calculate the GIC time series, GIC(t), required for transformer thermal impact assessment.

The geomagnetic latitude of the Ottawa geomagnetic observatory is 55°; therefore, the amplitude of the geomagnetic field measurement data were scaled up to the 60° reference geomagnetic latitude (see **Figure 1**) such that the resulting peak geoelectric field amplitude computed using the reference earth model was 8 V/km (see **Figures 2** and **3**). Sampling rate for the geomagnetic field waveshape is 10 seconds.

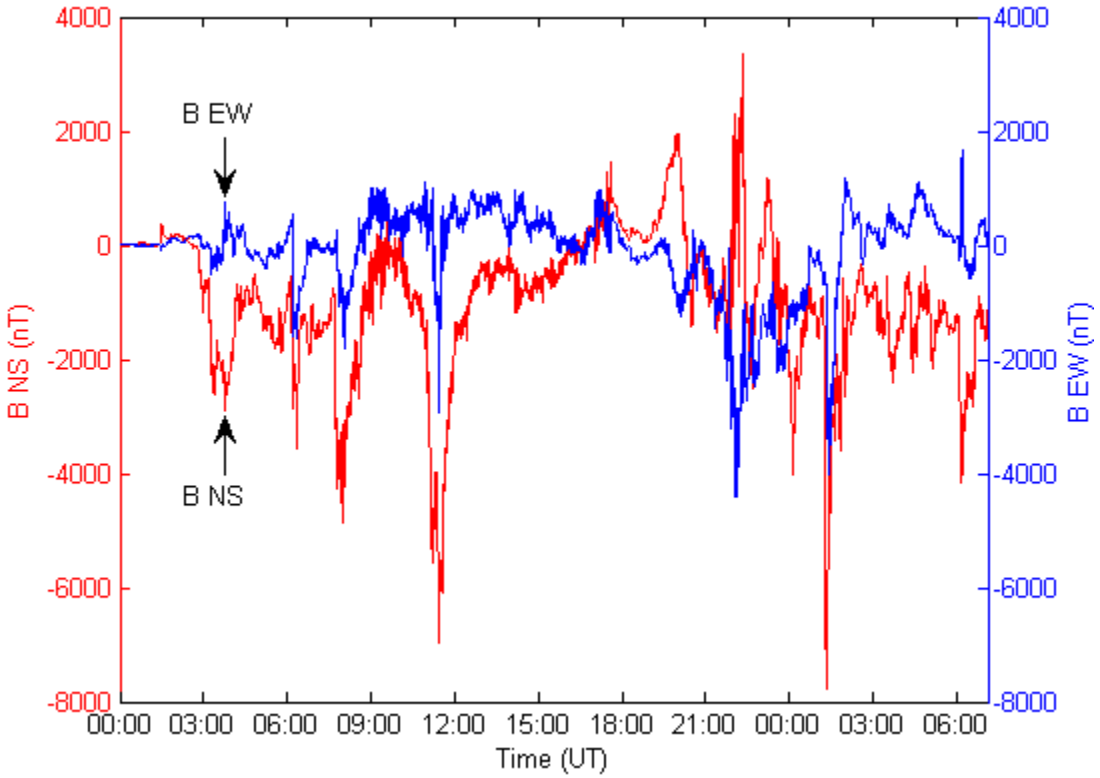

Figure 1: Benchmark Geomagnetic Field Waveshape
Red Bn (Northward), Blue Be (Eastward)
Referenced to pre-event quiet conditions

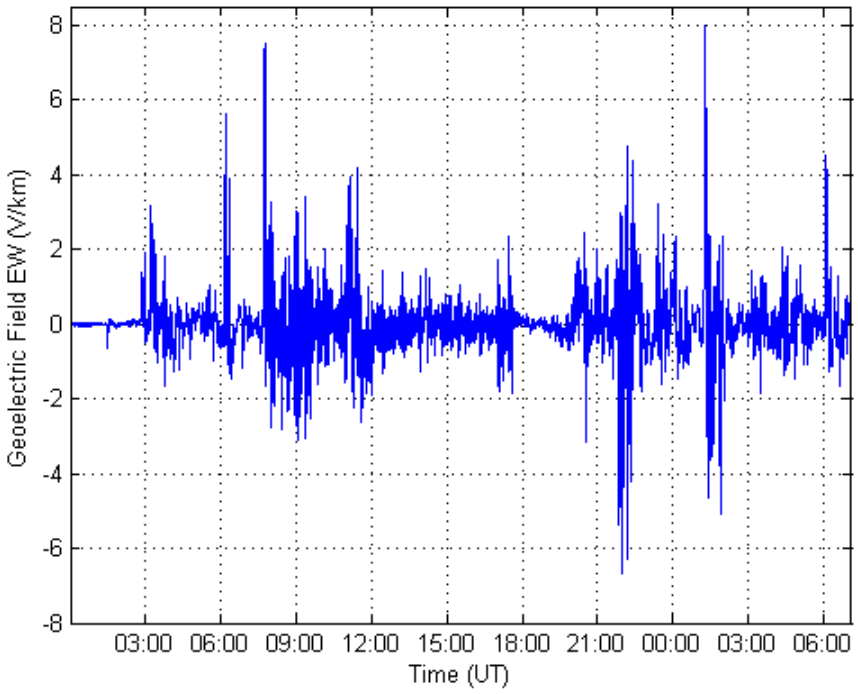

Figure 2: Benchmark Geoelectric Field Waveshape (E_E Eastward)

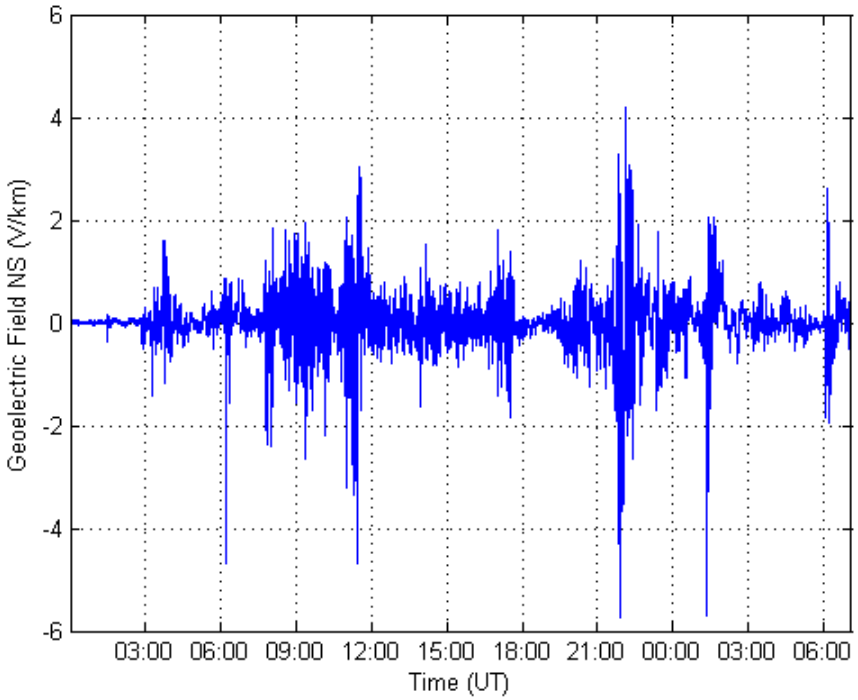

Figure 3: Benchmark Geoelectric Field Waveshape (E_N Northward)

Appendix I – Technical Considerations

The following sections describe the technical justification of the assumptions that were made in the development of the benchmark GMD event.

Statistical Considerations

Due to the lack of long-term accurate geomagnetic field observations, assigning probabilities to the occurrence of historical extreme geomagnetic storms is difficult because of the lack of high fidelity geomagnetic recordings of events prior to the 1980s. This is particularly true for the Carrington event for which data that allow the direct determination of the geoelectric fields experienced during the storm are not available [15].

The storm-time disturbance index Dst has often been used as a measure of storm strength even though it does not provide a direct correspondence with GIC[1]. One of the reasons for using Dst in statistical analysis is that Dst data are available for events occurring prior to 1980. Extreme value analysis of GMD events, including the Carrington, September 1859 and March 1989 events, has been carried out using Dst as an indicator of storm strength. In one such study [16], the (one sigma) range of 10-year occurrence probability for another March 1989 event was estimated to be between 9.4-27.8 percent. The range of 10-year occurrence probability for Carrington event in Love's analysis is 1.6-13.7 percent. These translate to occurrence rates of approximately 1 in 30-100 years for the March 1989 event and 1 in 70-600 years for the Carrington event. The error bars in such analysis are significant, however it is reasonable to conclude that statistically the March 1989 event is likely more frequent than 1-in-100 years and the Carrington event is likely less frequent than 1-in-100 years.

The benchmark GMD event is based on a 1 in 100 year frequency of occurrence which is a conservative design basis for power systems. Also, the benchmark GMD event is not biased towards local geomagnetic field enhancements since it must address wide-area effects in the interconnected power system. Therefore, the use of Dst-based statistical considerations is not adequate in this context and only relatively modern data have been used.

The benchmark GMD event is derived from modern geomagnetic field data records and corresponding calculated geoelectric field amplitudes. Using such data allows rigorous statistical analysis of the occurrence rates of the physical parameter (i.e. rate of change in geomagnetic field, dB/dt) directly related to the geoelectric field. Geomagnetic field measurements from the IMAGE magnetometer chain for 1993-2013 have been used to study the occurrence rates of the geoelectric field amplitudes.

With the use of modern data it is possible to avoid bias caused by localized geomagnetic field enhancements. The spatial structure of high-latitude geoelectric fields can be very complex during strong geomagnetic storm events [17]-[18]. One reflection of this spatial complexity is localized geomagnetic field enhancements that result in high amplitude geoelectric fields in regions of a few hundred kilometers or less. **Figure I-1**[2] illustrates this spatial complexity of the storm-time geoelectric fields. In areas indicated by the bright red location, the geoelectric field can be a factor of 2-3 larger than at neighboring locations. Localized geomagnetic phenomena should not be confused with local earth structure/conductivity features that result in consistently high geoelectric fields (e.g., coastal effects). Localized field enhancements can occur at any region exposed to auroral ionospheric electric current fluctuations.

[1] Dst index quantifies the amplitude of the main phase disturbance of a magnetic storm. The index is derived from magnetic field variations recorded at four low-latitude observatories. The data is combined to provide a measure of the average main-phase magnetic storm amplitude around the world.

[2] **Figure I-1** is for illustration purposes only, and is not meant to suggest that any one area is more likely to experience a localized enhanced geoelectric field.

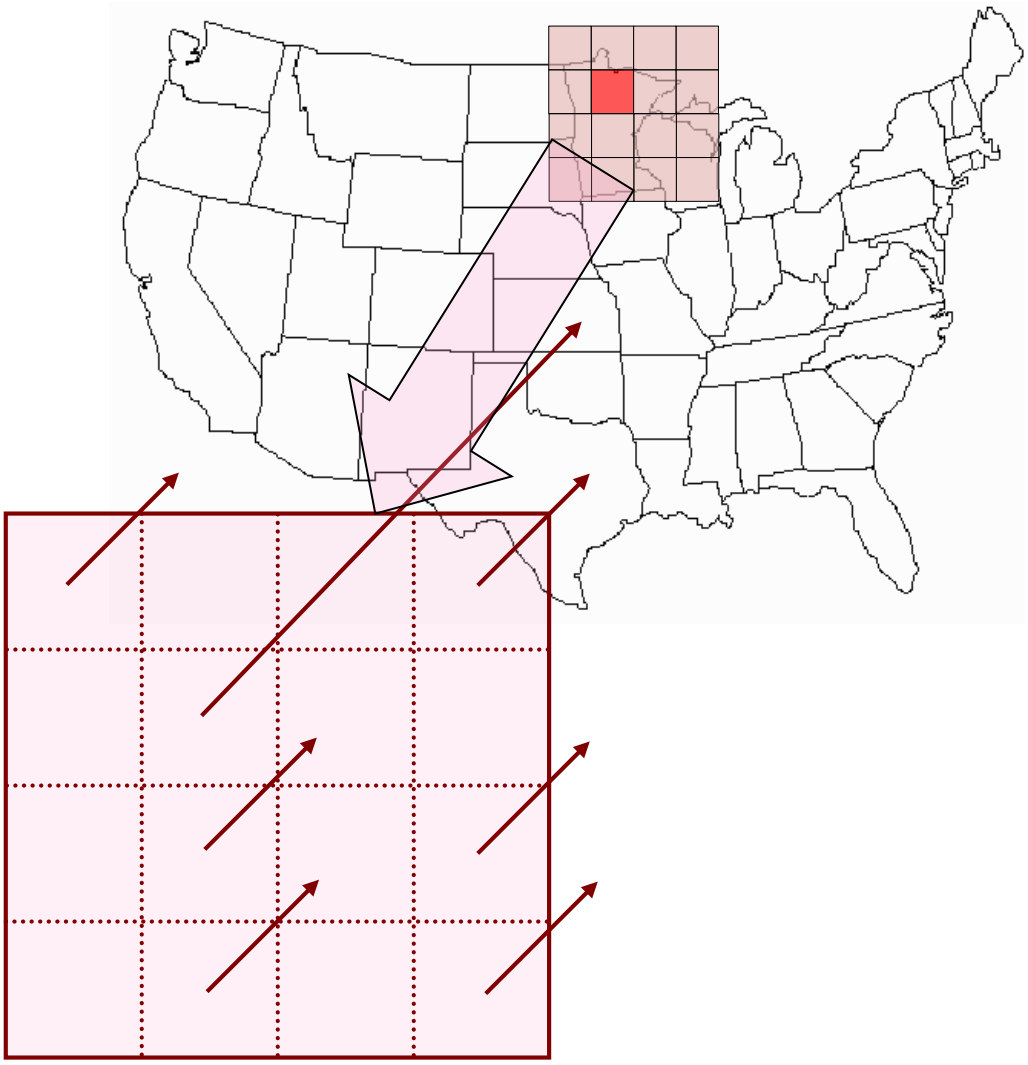

Figure I-1: Illustration of the Spatial Scale between Localized Enhancements and Larger Spatial Scale Amplitudes of Geoelectric Field Observed during a Strong Geomagnetic Storm.
In this illustration, the red square illustrates a spatially localized field enhancement.

The benchmark event is designed to address wide-area effects caused by a severe GMD event, such as increased var absorption and voltage depressions. Without characterizing GMD on regional scales, statistical estimates could be weighted by local effects and suggest unduly pessimistic conditions when considering cascading failure and voltage collapse. It is important to note that most earlier geoelectric field amplitude statistics and extreme amplitude analyses have been built for individual stations thus reflecting only localized spatial scales [10], [19]-[22]. A modified analysis is required to account for geoelectric field amplitudes at larger spatial scales. Consequently, analysis of spatially averaged geoelectric field amplitudes is presented below.

Figure I-2 shows statistical occurrence of spatially averaged high latitude geoelectric field amplitudes for the period of January 1, 1993 – December 31, 2013. The geoelectric field amplitudes were calculated using 10-s IMAGE magnetometer array observations and the Quebec ground conductivity model, which is used as a reference in the benchmark GMD event. Spatial averaging was carried out over four different station groups spanning a square area of approximately 500 km in width. For the schematic situation in **Figure I-1** the averaging process involves taking the average of the geoelectric field amplitudes over all 16 points or squares.

As can be seen from **Figure I-2**, the computed spatially averaged geoelectric field amplitude statistics indicate the 1-in-100 year amplitude is approximately between 3-8 V/km. Using extreme value analysis as described in the next section, it can be shown that the upper limit of the 95% confidence interval for a 100-year return level is more precisely 5.77 V/km.

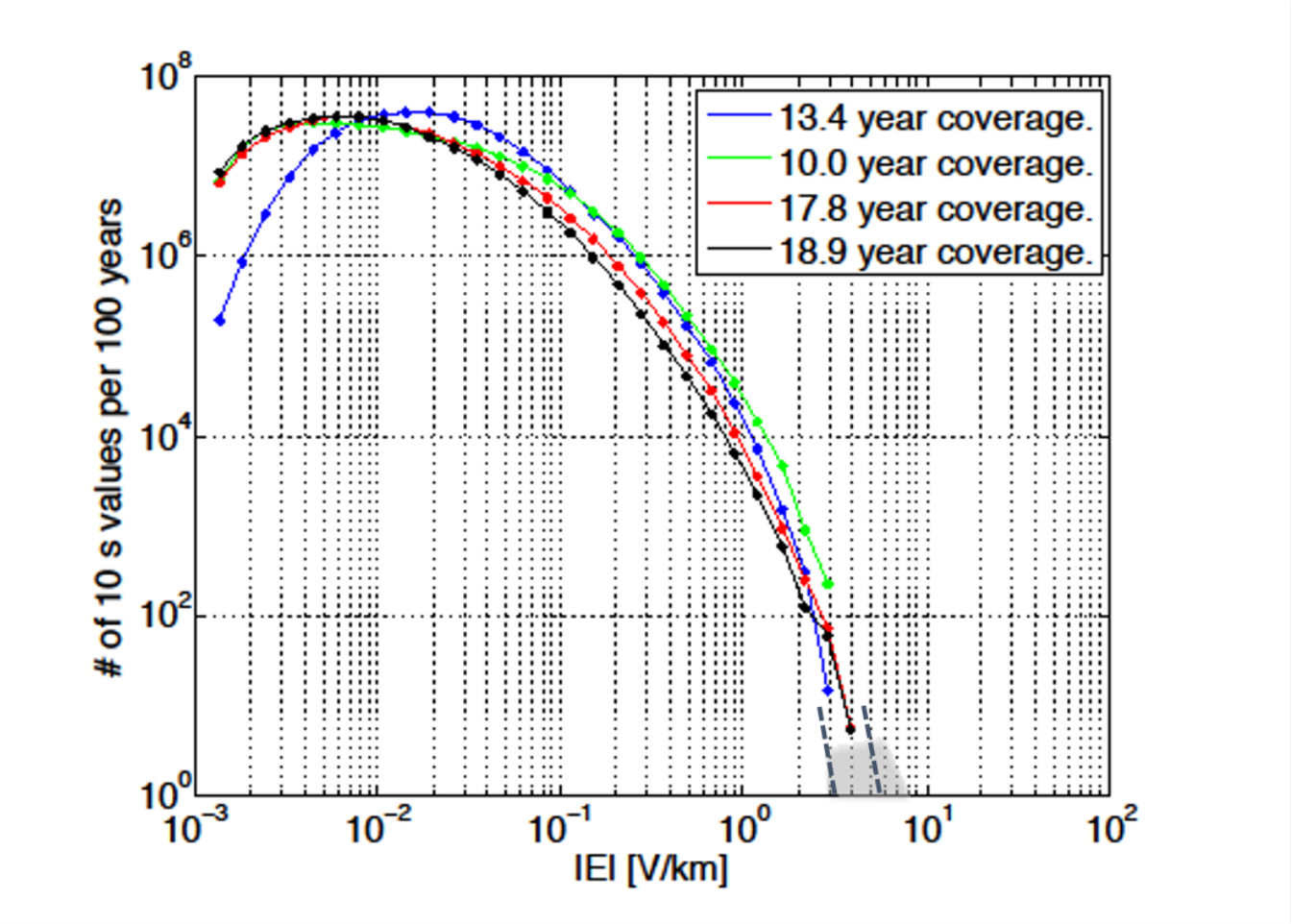

Figure I-2: Statistical Occurrence of Spatially Averaged Geoelectric Field Amplitudes.
Four curves with dots correspond to different station groups and the gray area shows a visual extrapolation to 1-in-100 year amplitudes. Dashed lines represent the values predicted with extreme value analysis. The legend shows the data coverage for each station group used in computing the averaged geoelectric field amplitudes.

Extreme Value Analysis

The objective of extreme value analysis is to describe the behavior of a stochastic process at extreme deviations from the median. In general, the intent is to quantify the probability of an event more extreme than any previously observed. In particular, we are concerned with estimating the 95 percent confidence interval of the maximum geo-electric field amplitude to be expected within a 100-year return period.[3] In the context of this document, extreme value analysis has been used to rigorously support the extrapolation estimates used in the statistical considerations of the previous section.

The data set consists of 21 years of daily maximum geoelectric field amplitudes derived from the IMAGE magnetometer chain, using the Quebec earth model as reference. **Figure I-3** shows a scatter plot of the 10-largest geoelectric field amplitudes per year across the IMAGE stations. The plot indicates that both the amplitude and standard deviation of extreme geoelectric fields are not independent of the solar cycle. The data clearly exhibits heteroskedasticity[4] and an 11-year seasonality in the mean.

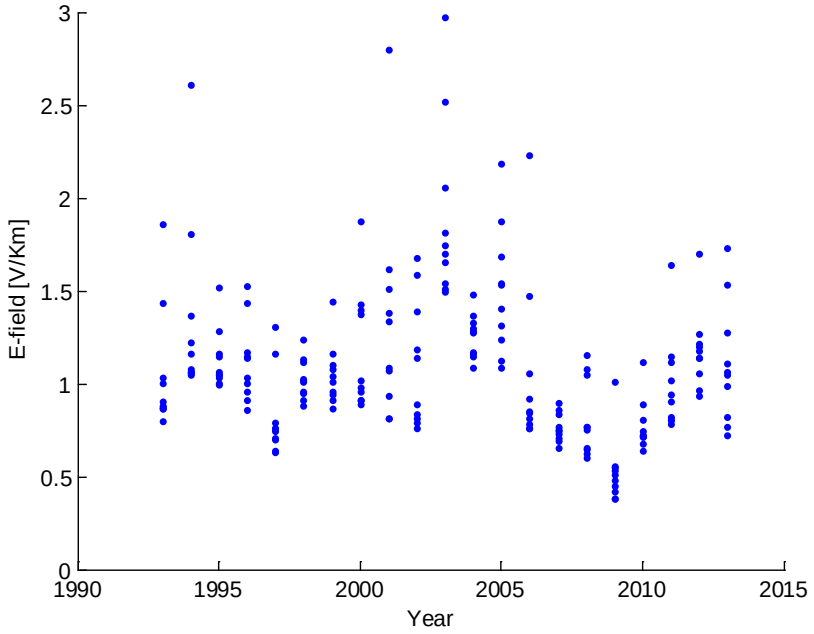

Figure I-3: Scatter Plot of Ten Largest Geoelectric Fields per Year

Data source: IMAGE magnetometer chain from 1993-2013

Several statistical methods can be used to conduct extreme value analysis. The most commonly applied include: Generalized Extreme Value (GEV), Point Over Threshold (POT), R-Largest, and Point Process (PP). In general, all methods assume independent and identically distributed (iid) data [23].

Two of these methods, GEV and POT, have been applied to the geoelectric field data, and their suitability for this application has been examined. **Table I-1** shows a summary of the estimated parameters and return levels obtained from GEV and POT methods. The parameters were estimated using the Maximum Likelihood Estimator (MLE). Since the distribution parameters do not have an intuitive interpretation, the expected geoelectric field amplitude for a 100-year return period is also included in **Table I-1.** The 95 percent confidence interval of the 100-year return level was calculated using the delta method and the profile likelihood. The delta method relies on the

[3] A 95 percent confidence interval means that, if we were to obtain repeated samples, the return level would lie within the confidence interval for 95 percent of the samples.

[4] Heteroskedasticity means that the skedastic function depends on the values of the conditioning variable; i.e., *var(Y|X=x) = f(x)*.

Gaussian approximation to the distribution of the MLE; this approximation can be poor for long return periods. In general, the profile likelihood provides a better description of the return level.

Table I-1: Extreme Value Analysis

Statistical Method	Estimated Parameters	Hypothesis Testing	100 Year Return Level Mean [V/km]	95% CI [V/km]	95% CI P-Likelihood [V/km]
(1) GEV	μ=1.4499 (0.1090) σ=0.4297 (0.0817) ξ=0.0305 (0.2011)	H0: ξ=0 *p* = 0.877	3.57	[1.77 , 5.36]	[2.71, 10.26]
(2) GEV $\mu = \beta_0 + \beta_1 \cdot \sin\left(\frac{t}{T} + \phi\right)$	β_0=1.5047 (0.0753) β_1=0.3722 (0.0740) σ=0.2894 (0.0600) ξ=0.1891 (0.2262)	H0: β_1=0 *p*= 0.0003 H0: ξ=0 *p* = 0.38	4	[2.64, 4.81]	[2.92, 12.33]
(3) POT, threshold=1V/km	σ=0.3163 (0.0382) ξ=0.0430 (0.0893)		3.4	[2.28, 4.52]	[2.72,5.64]
(4) POT, threshold=1V/km $\sigma = \alpha_0 + \alpha_1 \cdot \sin\left(\frac{t}{T} + \phi\right)$	α_0=0.2920 (0.0339) α_1=0.1660 (0.0368) ξ=-0.0308 (0.0826)	H0: α_1=0 *p*= 3.7e-5	3.724	[2.64, 4.81]	[3.02, 5.77]

Statistical model (1) in **Table I-1** is the traditional GEV estimation using blocks of 1 year maxima; i.e., only 21 data points are used in the estimation. The mean expected amplitude of the geolectric field for a 100-year return level is 3.57 V/km. Since GEV works with blocks of maxima, it is typically regarded as a wasteful approach. This is reflected in the comparatively large confidence intervals: [1.77, 5.36] V/km for the delta method and [2.71, 10.26] V/km for the profile likelihood.

As discussed previously, GEV assumes that the data is iid. Based on the scatter plot shown in **Figure 1-3**, the iid statistical assumption is not warranted by the data. Statistical model (2) in **Table I-1** is a re-parameterization of the GEV distribution contemplating the 11-year seasonality in the mean,

$$\mu = \beta_0 + \beta_1 \cdot \sin\left(\frac{t}{T} + \phi\right)$$

where β_0 represents the offset in the mean, β_1 describes the 11-year seasonality, *T* is the period (11 years), and ϕ is a constant phase shift.

A likelihood ratio test is used to test the hypothesis that β_1 is zero. The null hypothesis, H0: β_1=0, is rejected with a p-value of 0.0003; as expected, the 11-year seasonality has explanatory power. The blocks of maxima during the solar minimum are better represented in the re-parameterized GEV. The benefit is an increase in the mean return

level to 4 V/km and a wider confidence interval: [2.63, 4.81] V/km for the delta method and [2.92, 12.33] V/km for the profile likelihood (calculated at solar maximum).

Statistical model (3) in **Table I-1** is the traditional POT estimation using a threshold *u* of 1 V/km; the data was de-clustered using a 1-day run. The data set consists of normalized excesses over a threshold, and therefore, the sample size for POT is increased if more than one extreme observation per year is available (in the GEV approach, only the maximum observation over the year was taken; in the POT method, a single year can have multiple observations over the threshold). The selection of the threshold *u* is a compromise between bias and variance. The asymptotic basis of the model relies on a high threshold; a threshold that is too low will likely lead to bias. On the other hand, a threshold that is too high will reduce the sample size and result in high variance. The stability of parameter estimates can guide the selection of an appropriate threshold. **Figure I-4** shows the estimated parameters (modified scale $\sigma^*=\sigma_u-\xi\cdot u$, and shape ξ) for a range of thresholds. The objective is to select the lowest threshold for which the estimates remain near constant; 1V/km appears to be a good choice.

The mean return level for statistical model (3), 3.4 V/km, is similar to the GEV estimates. However, due to the larger sample size the POT method is more efficient, and consequently, the confidence intervals are significantly reduced: [2.28, 4.52] V/km for the delta method, and [2.72, 5.64] V/km for the profile likelihood method.

In order to cope with the heteroskedasticity exhibited by the data, a re-parameterization of POT is used in statistical model (4) in **Table I-1**,

$$\sigma = \alpha_0 + \alpha_1 \cdot \sin\left(\frac{t}{T} + \phi\right)$$

where α_0 represents the offset in the standard deviation, α_1 describes the 11-year seasonality, *T* is the period ($365.25 \cdot 11$), and ϕ is a constant phase shift.

The parameter α_1 is statistical significant; the null hypothesis, H0: $\alpha_1=0$, is rejected with a p-value of 3.7e-5. The mean return level has slightly increased to 3.72 V/km. The upper limit of the confidence interval, calculated at solar maximum, also increases: [2.63, 4.81] V/km for the delta method and [3.02, 5.77] V/km for the profile likelihood method. As a final remark, it is emphasized that the confidence interval obtained using the profile likelihood is preferred over the delta method. **Figure I-5** shows the profile likelihood of the 100-year return level of statistical model (4). Note that the profile likelihood is highly asymmetric with a positive skew, rendering a larger upper limit for the confidence interval. Recall that the delta method assumes a normal distribution for the MLEs, and therefore, the confidence interval is symmetric around the mean.

To conclude, traditional GEV (1) and POT (3) models are misspecified; the statistical assumptions (iid) are not warranted by the data. The models were re-parameterized to cope with heteroskedasticity and the 11-year seasonality in the mean. Statistical model (4) better utilizes the available extreme measurements and it is therefore preferred over statistical model (2). The upper limit of the 95 percent confidence interval for a 100-year return level is 5.77 V/km. This analysis shows that the geoelectric field amplitude of 8 V/km for the benchmark is conservative for a 100-year return level and it includes an implicit 25 percent engineering margin.

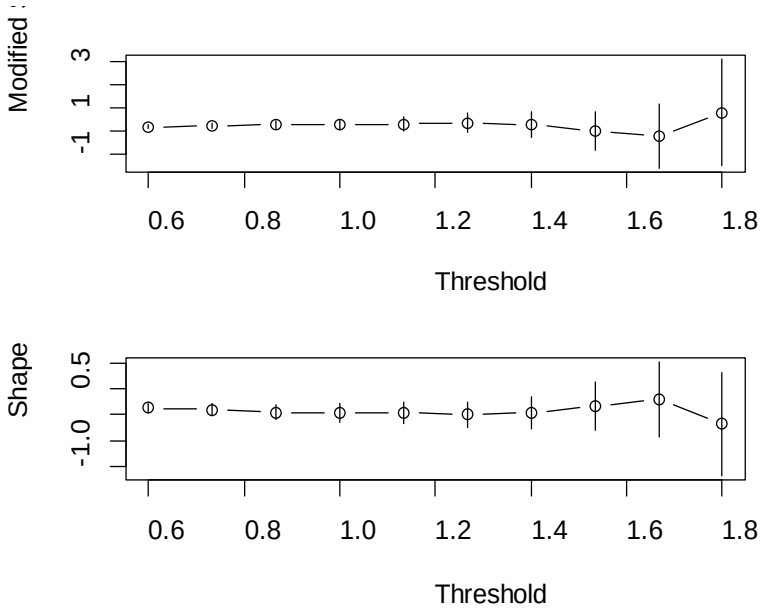

Figure I-4: Parameter Estimates Against Threshold for Statistical Model (3)

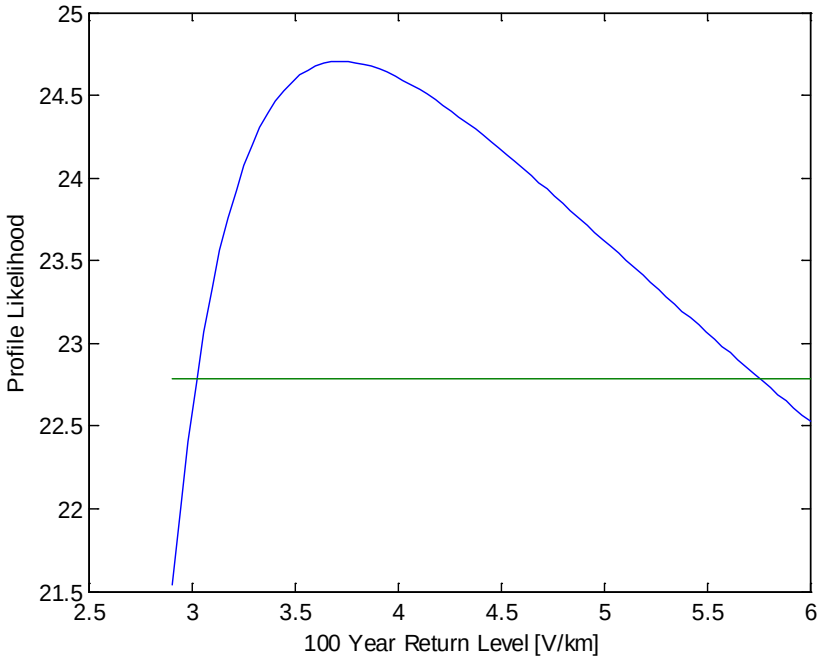

Figure I-5: Profile Likelihood for 100-year Return Level for Statistical Model (4)

Impact of Local Geomagnetic Disturbances on GIC

The impact of local disturbances on a power network is illustrated with the following example. A 500 km by 500 km section of a North American transmission network is subdivided into 100 km by 100 km sections. The geoelectric field is assumed to be uniform within each section. The analysis is performed by scaling the geoelectric field in each section individually by an intensification factor of 2.5 and computing the corresponding GIC flows in the network, resulting in a total of 25 GIC distribution simulations.[5] In these simulations the peak geomagnetic field amplitude has been scaled according to geomagnetic latitude of the network under study.

Figure I-6 shows the number of transformers that experience a GIC increase greater than 10 Amps (in red), those that experienced a reduction in GIC of more than 10 Amps (in blue), and those that remain essentially the same (in green). It can be observed that there is a small set of transformers that are affected by the local amplification of the geo-electric field but that the impact on the GIC distribution of the entire network due to a local intensification of the geoelectric field in a "local peak" is minor. Therefore, it can be concluded that the effect of local disturbances on the larger transmission system is relatively minor and does not warrant further consideration in network analysis.

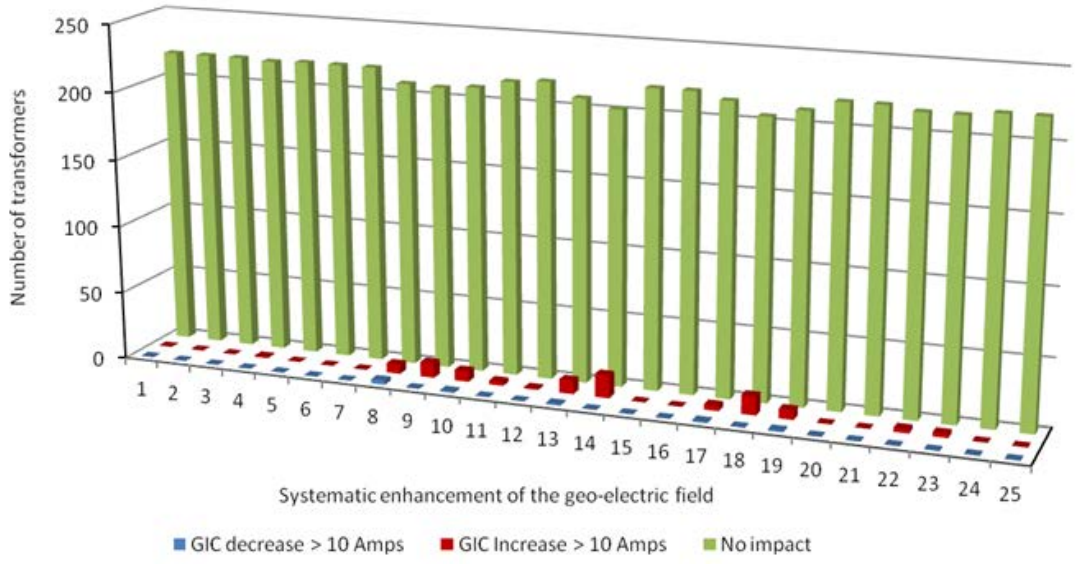

Figure I-6: Number of Transformers that see a 10 A/phase Change in GIC due to Local Geoelectric Field Intensification

Impact of Waveshape on Transformer Hot-spot Heating

Thermal effects (e.g. hot spot transformer heating) in power transformers are not instantaneous. Thermal time constants associated with hot spot heating in power transformers are in the 5-20 minute range; therefore, the waveshape of the geomagnetic and geoelectric field has a strong impact on transformer hot spot heating of windings and metallic parts since thermal time constants are of the same order of magnitude as the time-to-peak of storm maxima. The waveshape of the March 13-14 1989 GMD event measured at the Ottawa geomagnetic observatory was found to be a conservative choice when compared with other events of the last 20 years, such

[5] An intensification factor of 2.5 would make a general 8 V/km peak geoelectric field in the entire network show a 20 V/km intensified geoelectric field in one of the twenty five 100 km by 100 km sections.

as the reference storm of the NERC interim report of 2012 [14], measurements at the Nurmijarvi (NUR) and Memanbetsu (MMB) geomagnetic observatories for the "Halloween event" of October 29-31, 2003.

To illustrate, the results of a thermal analysis performed on a relatively large test network with a diverse mix of circuit lengths and orientations is provided in **Figures I-7** and **I-8**. These results illustrate the relative effect of different waveshapes in a broad system setting and should not be interpreted as a vulnerability assessment of any particular network.

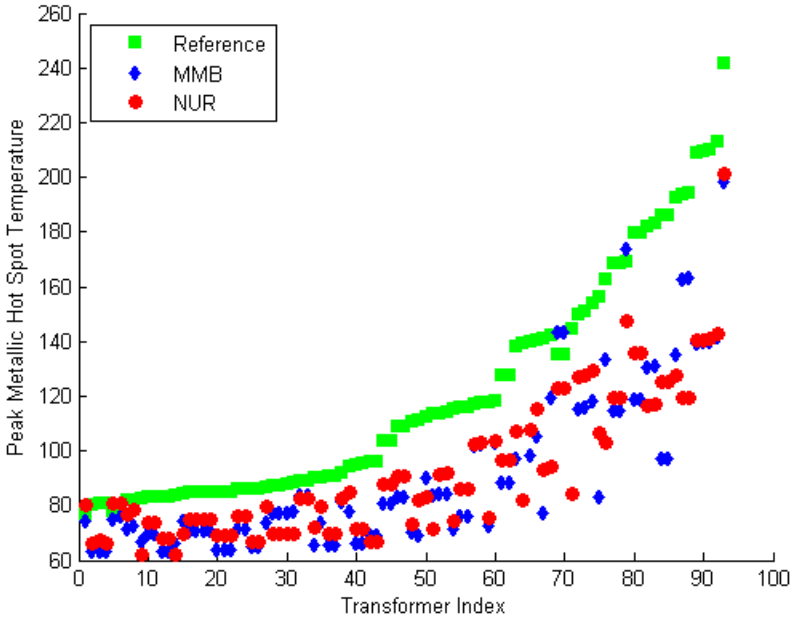

Figure I-7: Calculated Peak Metallic Hot Spot Temperature for All Transformers in a Test System with a Temperature Increase of More Than 20°C for Different GMD Events Scaled to the Same Peak Geoelectric Field

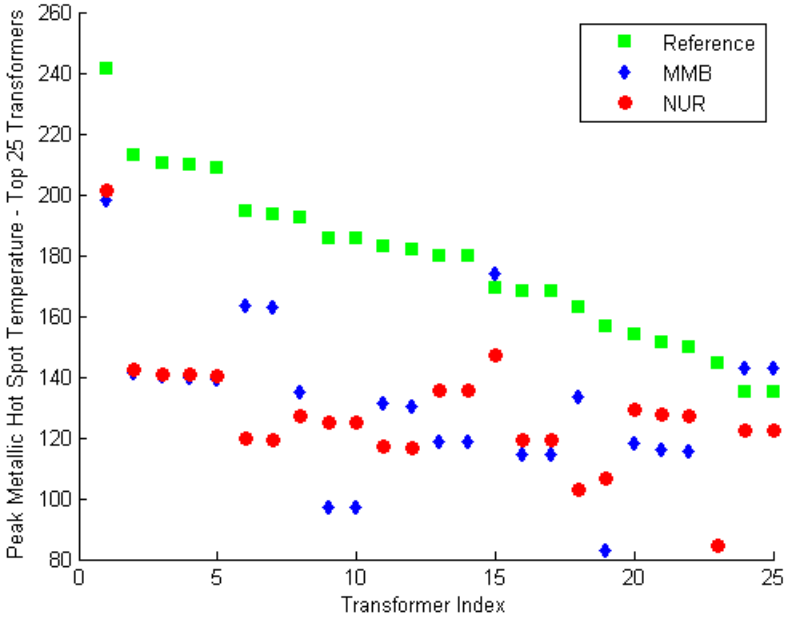

Figure I-8: Calculated Peak Metallic Hot Spot Temperature for the Top 25 Transformers in a Test System for Different GMD Events Scaled to the Same Peak Geoelectric Field

Appendix II – Scaling the Benchmark GMD Event

The intensity of a GMD event depends on geographical considerations such as geomagnetic latitude[6] and local earth conductivity[7] [3]**.** Scaling factors for geomagnetic latitude take in consideration that the intensity of a GMD event varies according to latitude-based geographical location. Scaling factors for earth conductivity take into account that the induced geoelectric field depends on earth conductivity, and that different parts of the continent have different earth conductivity and deep earth structure.

Scaling the Geomagnetic Field

The benchmark GMD event is defined for geomagnetic latitude of 60° and it must be scaled to account for regional differences based on geomagnetic latitude. To allow usage of the reference geomagnetic field waveshape in other locations, **Table II-1** summarizes the scaling factor α correlating peak geoelectric field to geomagnetic latitude as described in **Figure II-1** [3]. This scaling factor α has been obtained from a large number of global geomagnetic field observations of all major geomagnetic storms since the late 1980s [15], [24]-[25], and can be approximated with the empirical expression in (II.1)

$$\alpha = 0.001 \cdot e^{(0.115 \cdot L)} \qquad \text{(II.1)}$$

where L is the geomagnetic latitude in degrees and $0.1 \leq \alpha \leq 1.0$.

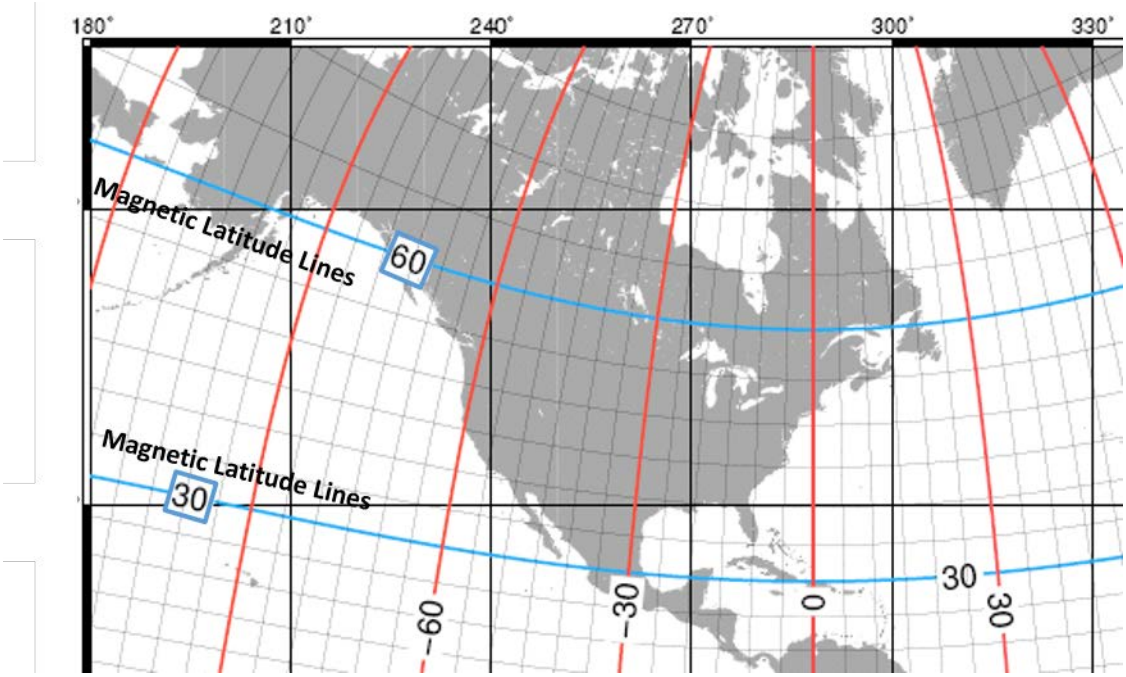

Figure II-1: Geomagnetic Latitude Lines in North America

[6] Geomagnetic latitude is analogous to geographic latitude, except that bearing is in relation to the magnetic poles, as opposed to the geographic poles. Geomagnetic phenomena are often best organized as a function of geomagnetic coordinates.

[7] Local earth conductivity refers to the electrical characteristics to depths of hundreds of km down to the earth's mantle. In general terms, lower ground conductivity results in higher geoelectric field amplitudes.

Table II-1: Geomagnetic Field Scaling Factors	
Geomagnetic Latitude (Degrees)	Scaling Factor1 (α)
≤ 40	0.10
45	0.2
50	0.3
54	0.5
56	0.6
57	0.7
58	0.8
59	0.9
≥ 60	1.0

Scaling the Geoelectric Field

The benchmark GMD event is defined for the reference Quebec earth model provided in **Table 1**. This earth model has been used in many peer-reviewed technical articles [12, 15]. The peak geoelectric field depends on the geomagnetic field waveshape and the local earth conductivity. Ideally, the peak geoelectric field, E_{peak}, is obtained by calculating the geoelectric field from the scaled geomagnetic waveshape using the plane wave method and taking the maximum value of the resulting waveforms

$$E_N = (z(t)/\mu_o) * B_E(t)$$
$$E_E = -(z(t)/\mu_o) * B_N(t) \qquad \text{(II.2)}$$
$$E_{peak} = \max\left\{\left|E_E(t), E_N(t)\right|\right\}$$

where,

* denotes convolution in the time domain,

z(t) is the impulse response for the earth surface impedance calculated from the laterally uniform or 1D earth model,

$B_E(t)$, $B_N(t)$ are the scaled Eastward and Northward geomagnetic field waveshapes,

$E_E(t)$, $E_N(t)|$ are the magnitudes of the calculated Eastward and Northward geoelectric field $E_E(t)$ and $E_N(t)$.

As noted previously, the response of the earth to B(t) (and dB/dt) is frequency dependent. **Figure II-2** shows the magnitude of Z(ω) for the reference earth model.

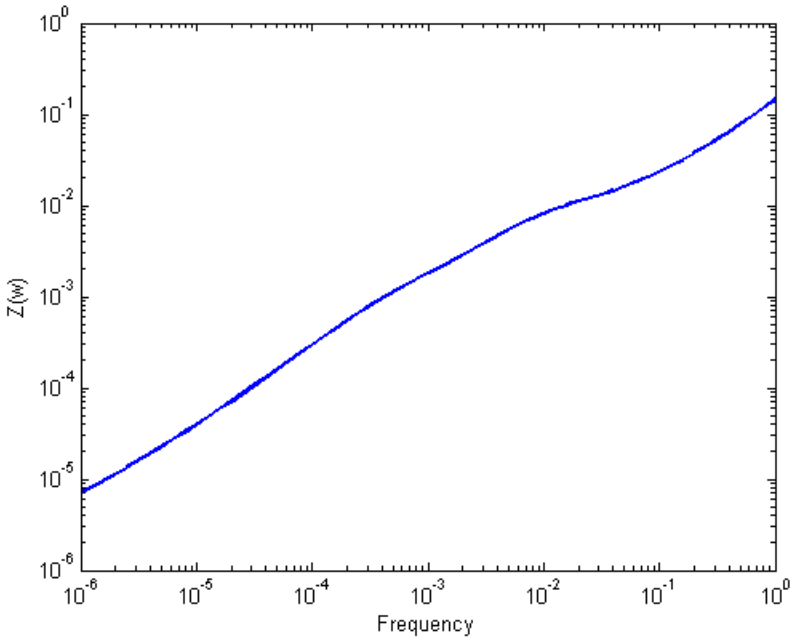

Figure II-2: Magnitude of the Earth Surface Impedance for the Reference Earth Model

If a utility does not have the capability of calculating the waveshape or time series for the geoelectric field, an earth conductivity scaling factor β can be obtained from **Table II-2**. Using α and β, the peak geoelectric field E_{peak} for a specific service territory shown in **Figure II-3** can be obtained using (II.3)

$$E_{peak} = 8 \times \alpha \times \beta \text{ (V/km)} \quad \text{(II.3)}$$

It should be noted that (II.3) is an approximation based on the following assumptions:

- The earth models used to calculate Table II-2 for the United States are from magnetotelluric data and are available from the USGS website.
- The models used to calculate Table II-2 for Canada were obtained from NRCan and reflect the average structure for large regions. When models are developed for sub-regions these will all be different (to a greater or lesser degree) from the average model. For instance, detailed models for Ontario have been developed by NRCan and consist of seven major sub-regions.
- The conductivity scaling factor β is calculated as the quotient of the local geoelectric field peak amplitude in a physiographic region with respect to the reference peak amplitude value of 8 V/km. Both geoelectric field peaks amplitudes are calculated using the reference geomagnetic field time series. If a different geomagnetic field time series were used, the calculated scaling factors β would be different than the values in Table II-2 because the frequency content of storm maxima is, in principle, different for every storm. However, the reference time series produces generally more conservative values of β when compared to the time series of reference storm of the NERC interim report of 2012 [14], measurements at the Nurmijarvi (NUR) and Memanbetsu (MMB) geomagnetic observatories for the "Halloween event" of October 29-31, 2003, and other recordings of the March 1989 event at high latitudes (Meanook observatory, Canada). The average variation between minimum and maximum β is approximately 12 percent. **Figure II-4** illustrates the values of β calculated using the 10-second recordings for these geomagnetic field time series.
- If a utility has technically-sound earth models for its service territory and sub-regions thereof, then the use of such earth models is preferable to estimate E_{peak}.

- When a ground conductivity model is not available the planning entity should use a β factor of 1 or other technically-justified value.

Physiographic Regions of the Continental United States

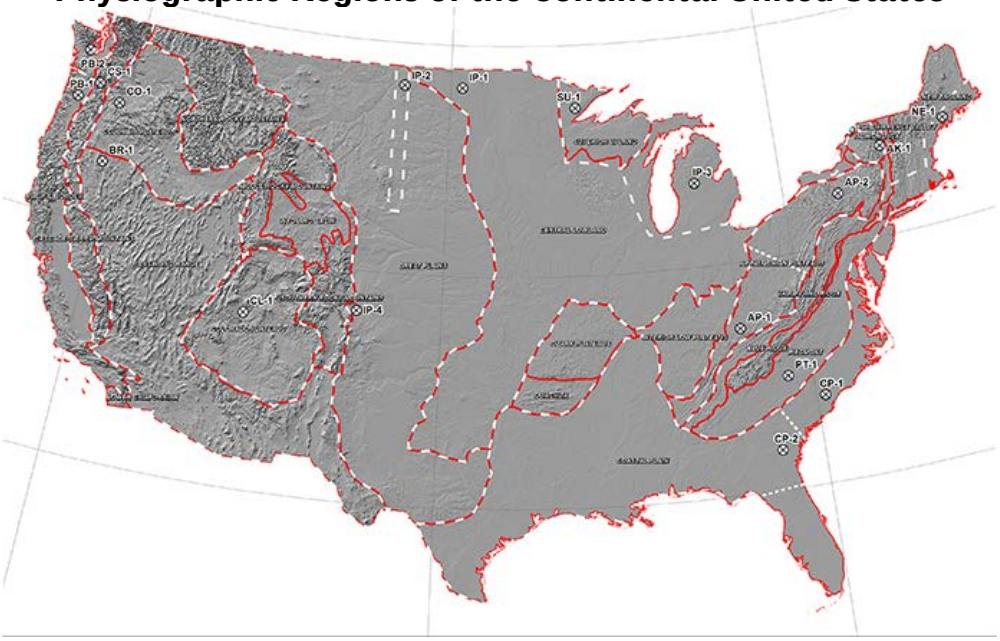

Physiographic Regions of Canada

Figure II-3: Physiographic Regions of North America

Table II-2 Geoelectric Field Scaling Factors	
USGS Earth model	Scaling Factor (β)
AK1A	0.56
AK1B	.0.56
AP1	0.33
AP2	0.82
BR1	0.22
CL1	0.76
CO1	0.27
CP1	0.81
CP2	0.95
CS1	0.41
IP1	0.94
IP2	0.28
IP3	0.93
IP4	0.41
NE1	0.81
PB1	0.62
PB2	0.46
PT1	1.17
SL1	0.53
SU1	0.93
BOU	0.28
FBK	0.56
PRU	0.21
BC	0.67
PRAIRIES	0.96
SHIELD	1.0
ATLANTIC	0.79

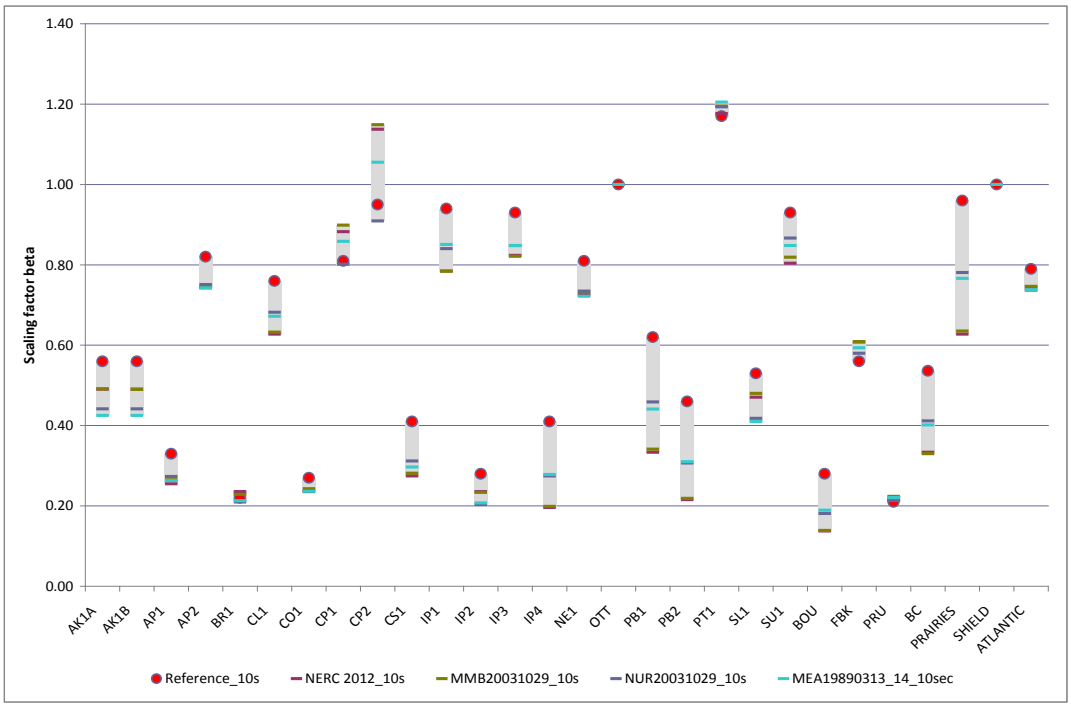

Figure II-4: Beta factors Calculated for Different GMD Events
Red circles corresponds to the values in Table II-2

Example Calculations

Example 1

Consider a transmission service territory that lies in a geographical latitude of 45.5°, which translates to a geomagnetic latitude of 55°. The scaling factor α calculated using II.1 is 0.56; therefore, the benchmark waveshape and the peak geoelectric field will be scaled accordingly. If the service territory has the same earth conductivity as the benchmark then β=1, and the peak geoelectric field will be

$$\alpha = 0.56$$
$$\beta = 1.0$$
$$E_{peak} = 8 \times 0.56 \times 1 = 4.5 V / km$$

If the service territory spans more than one physiographic region (i.e. several locations within the service territory have a different earth model) then the largest α can be used across the entire service territory for conservative results. Alternatively, the network can be split into multiple subnetworks, and the corresponding geoelectric field amplitude can be applied to each subnetwork.

Example 2

Consider a service territory that lies in a geographical latitude of 45.5° which translates to a geomagnetic latitude of 55°. The scaling factor α calculated using II.1 is 0.56; therefore, the benchmark waveshape and the peak geoelectric field will be scaled accordingly.

The service territory has lower conductivity that the reference benchmark conductivity, and according to the conductivity factor β from Table II-2. Then:

Conductivity factor β=1.17

$$\alpha = 0.56$$

$$E_{peak} = 8 \times 0.56 \times 1.17 = 5.2V / km$$

References

[1] L. Bolduc, A. Gaudreau, A. Dutil, "Saturation Time of Transformers Under dc Excitation", Electric Power Systems Research, 56 (2000), pp. 95-102

[2] *High-Impact, Low-Frequency Event Risk to the North American Bulk Power System*, A Jointly-Commissioned Summary Report of the North American Reliability Corporation and the U.S. Department of Energy's November 2009 Workshop.

[3] Application Guide: Computing Geomagnetically-Induced Current in the Bulk-Power System, NERC. NERC. http://www.nerc.com/comm/PC/Geomagnetic%20Disturbance%20Task%20Force%20GMDTF%202013/GIC%20Application%20Guide%202013_approved.pdf

[4] Kuan Zheng, Risto Pirjola, David Boteler, Lian-guang Liu, "Geoelectric Fields Due to Small-Scale and Large-Scale Source Currents", *IEEE Transactions on Power Delivery*, Vol. 28, No. 1, January 2013, pp. 442-449.

[5] Boteler, D. H. "Geomagnetically Induced Currents: Present Knowledge and Future Research", *IEEE Transactions on Power Delivery*, Vol. 9, No. 1, January 1994, pp. 50-58.

[6] Boteler, D. H. "Modeling Geomagnetically Induced Currents Produced by Realistic and Uniform Electric Fields", *IEEE Transactions on Power Delivery*, Vol. 13, No. 4, January 1998, pp. 1303-1308.

[7] J. L. Gilbert, W. A. Radasky, E. B. Savage, "A Technique for Calculating the Currents Induced by Geomagnetic Storms on Large High Voltage Power Grids", Electromagnetic Compatibility (EMC), 2012 IEEE International Symposium on.

[8] *How to Calculate Electric Fields to Determine Geomagnetically-Induced Currents.* EPRI, Palo Alto, CA: 2013. 3002002149.

[9] Pulkkinen, A., R. Pirjola, and A. Viljanen, Statistics of extreme geomagnetically induced current events, Space Weather, 6, S07001, doi:10.1029/2008SW000388, 2008.

[10] Boteler, D. H., Assessment of geomagnetic hazard to power systems in Canada, Nat. Hazards, 23, 101–120, 2001.

[11] Finnish Meteorological Institute's IMAGE magnetometer chain data available at: http://image.gsfc.nasa.gov/

[12] Boteler, D. H., and R. J. Pirjola, The complex-image method for calculating the magnetic and electric fields produced at the surface of the Earth by the auroral electrojet, Geophys. J. Int., 132(1), 31—40, 1998

[13] ANSI Standard C2, *National Electric Safety Code*, 2012, ISBN 978-0-7381-6588-2

[14] 2012 Special Reliability Assessment Interim Report: Effects of Geomagnetic Disturbances on the Bulk Power System. NERC. February 2012. http://www.nerc.com/pa/RAPA/ra/Reliability%20Assessments%20DL/2012GMD.pdf

[15] Pulkkinen, A., E. Bernabeu, J. Eichner, C. Beggan and A. Thomson, Generation of 100-year geomagnetically induced current scenarios, *Space Weather*, Vol. 10, S04003, doi:10.1029/2011SW000750, 2012.

[16] Love, J., Credible occurrence probabilities for extreme geophysical events: Earthquakes, volcanic eruptions, magnetic storms, Geophysical Research Letters, Vol. 39, L10301, doi:10.1029/2012GL051431, 2012.

[17] Pulkkinen, A., A. Thomson, E. Clarke, and A. Mckay, April 2000 geomagnetic storm: ionospheric drivers of large geomagnetically induced currents, Annales Geophysicae, 21, 709-717, 2003.

[18] Pulkkinen, A., S. Lindahl, A. Viljanen, and R. Pirjola, Geomagnetic storm of 29–31 October 2003: Geomagnetically induced currents and their relation to problems in the Swedish high-voltage power transmission system, Space Weather, 3, S08C03, doi:10.1029/2004SW000123, 2005.

[19] Pulkkinen, A., R. Pirjola, and A. Viljanen, Statistics of extreme geomagnetically induced current events, Space Weather, 6, S07001, doi:10.1029/2008SW000388, 2008.

[20] Langlois, P., L. Bolduc, and M. C. Chouteau, Probability of occurrence of geomagnetic storms based on a study of the distribution of the electric field amplitudes measured in Abitibi, Québec, in 1993–1994, J. Geomagn. Geoelectr., 48, 1033–1041, 1996.

[21] Pulkkinen, A., R. Pirjola, and A. Viljanen, Statistics of extreme geomagnetically induced current events, Space Weather, 6, S07001, doi:10.1029/2008SW000388, 2008.

[22] Campbell, W. C., Observation of electric currents in the Alaska oil pipeline resulting from auroral electrojet current sources, Geophys. J. R. Astron. Soc., 61, 437–449, 1980.

[23] Coles, Stuart (2001). An Introduction to Statistical Modelling of Extreme Values. Springer.

[24] Ngwira, C., A. Pulkkinen, F. Wilder, and G. Crowley, Extended study of extreme geoelectric field event scenarios for geomagnetically induced current applications, Space Weather, Vol. 11, 121–131, doi:10.1002/swe.20021, 2013.

[25] Thomson, A., S. Reay, and E. Dawson. Quantifying extreme behavior in geomagnetic activity, Space Weather, 9, S10001, doi:10.1029/2011SW000696, 2011.